RESEARCH ARTICLE

Microvascular Breakdown Due to Retinal Neurodegeneration in Ataxias

Christopher A. Turski, MD,[1,2*] Gabrielle N. Turski, MD,[1,2] Jennifer Faber, MD,[2,3] Stefan J. Teipel, MD,[4,5] Frank G. Holz, MD,[1] Thomas Klockgether, MD,[2,3] and Robert P. Finger, MD[1]

[1]*Department of Ophthalmology, University of Bonn, Bonn, Germany*
[2]*German Center for Neurodegenerative Diseases (DZNE), Bonn, Germany*
[3]*Department of Neurology, University of Bonn, Bonn, Germany*
[4]*Department of Psychosomatic Medicine, University of Rostock, Rostock, Germany*
[5]*German Center for Neurodegenerative Diseases (DZNE), Rostock, Germany*

ABSTRACT: Background: Neurodegenerative ataxias are devastating disorders of the cerebellum and spinal cord, accompanied by death of retinal ganglion cells, leading to relentlessly progressive decline of motor coordination and permanent disability. Retinal microvascular affection has not yet been determined.

Objectives: The aim of this study is to assess whether retinal microvascular alterations occur and, if so, whether they are concurrent with or follow cell death in the retina in neurodegenerative diseases.

Methods: This study involves the cross-sectional observational study of 43 patients with ataxia and 43 controls enrolled from August 1, 2018, to September 30, 2020. The extent of ataxia was determined by the Scale for the Assessment and Rating of Ataxia. Changes in retinal vasculature were examined by optical coherence tomography angiography (OCT-A) and retinal cell and fiber density by OCT in ataxias concurrently.

Results: When comparing the ataxia cohort with healthy subjects, ataxia patients exhibited reduced vessel density in the radial peripapillary capillary (RPC) network ($P = 0.005$), capillary density inside the optic nerve head (cdONH) ($P < 0.001$), nasal superficial vascular plexus ($P = 0.03$) as well as reduced ganglion cell layer (GCL) volume ($P = 0.04$), and temporal peripapillary retinal nerve fiber layer thickness ($P = 0.04$). Mixed effect analysis modeling laterality confirmed these findings.

Conclusions: These findings demonstrate a distinct pattern of concurrent changes in vessel density of the retinal superficial vascular complex, encompassing the superficial vascular plexus, RPC network and cdONH, and retinal GCL volume, providing new insights into the ongoing degeneration in ataxias. Our findings may have relevance for design of novel therapeutic approaches for ataxias and possibly other neurodegenerative diseases. © 2021 The Authors. *Movement Disorders* published by Wiley Periodicals LLC on behalf of International Parkinson and Movement Disorder Society

Key Words: ataxia; retinal vessel density; retinal ganglion cells; retinal superficial vascular complex; optical coherence tomography angiography

***Correspondence to:** Dr. C.A. Turski, Department of Ophthalmology, University of Bonn, Ernst-Abbe-Strasse 2, 53127 Bonn, Germany; E-mail: christopher.turski@ukbonn.de; christopher.turski@dzne.de

Christopher A. Turski and Gabrielle N. Turski contributed equally to this study and should therefore be regarded as equivalent authors.

Relevant conflicts of interest/financial disclosures: None.

Funding agency: None.

Received: 26 May 2021; **Revised:** 9 August 2021; **Accepted:** 26 August 2021

Published online 17 September 2021 in Wiley Online Library (wileyonlinelibrary.com). DOI: 10.1002/mds.28791

Ataxias are neurodegenerative diseases affecting the cerebellum and spinal cord. Clinically, ataxias are characterized by progressive loss of balance, deficits in coordination, and deterioration of speech. Although the cause of ataxias is heterogeneous, a large portion of ataxias possess genetic origin. The genetic ataxias are grouped as dominantly inherited diseases and designated spinocerebellar ataxias (SCAs) and recessive diseases, the most frequent of which is Friedreich's ataxia (FRDA).[1] The most common SCAs, including SCA1, SCA3, and SCA6, are due to CAG repeat expansion mutations, resulting in the accumulation of abnormal proteins containing expanded polyglutamine tracts.[2] In addition, there are nongenetic sporadic ataxias, including multiple system

atrophy of cerebellar type (MSA-C). MSA-C is a sporadic adult-onset disease of unknown cause that manifests with various combinations of progressive ataxia and autonomic failure. MSA-C is defined by the presence of α-synuclein-positive oligodendroglial cytoplasmic inclusions.[3]

Optical coherence tomography (OCT) has been used to assess microstructural retinal changes in patients with degenerative ataxias focusing on the retinal nerve fiber layer (RNFL) and ganglion cell layer (GCL).[4-13] However, other ocular features, including the retinal microvasculature, have not yet been evaluated in ataxias. It is even more intriguing because it is not yet known whether microvascular alterations occur and, if so, whether they are concurrent or follow cell death in neurodegenerative diseases. Although it has been established that Alzheimer's disease (AD) is associated with β-amyloid angiopathy and vascular changes in the retina,[14-20] the time course of neuronal versus vascular changes in the retina or brain of AD patients is not known. Optical coherence tomography angiography (OCT-A) has become available for noninvasive, high-resolution, and three-dimensional imaging of the retinal and optic nerve head vasculature not requiring intravenous dye injection as compared to conventional retinal fluorescein angiography or indocyanine green angiography.[21] OCT-A produces visualization of the retinal vascular network by calculating signal change in consecutive cross-sectional OCT images captured at the same retinal location, using motion of cellular blood components as intrinsic contrast.[21]

Thus, to fill the current knowledge gap, we assessed the retina, including its vasculature, using OCT-A and ganglion cells using OCT in patients with degenerative ataxias with the aim of discovering whether vascular alterations occur and, if so, what the relationship is between vascular and cellular alterations in the retina, pursuing a novel concurrent imaging approach that could assist in identifying and monitoring these diseases.

Patients and Methods

Patients

The study was a cross-sectional observational study performed at the German Center for Neurodegenerative Diseases (DZNE) in Bonn, Germany, in collaboration with the Department of Ophthalmology and the Department of Neurology of the University of Bonn, Bonn, Germany. The study was approved by the Institutional Review Board of the University of Bonn, Germany, and all procedures adhered to the tenets of the Declaration of Helsinki. Informed consent was obtained from all participants before enrollment between August 1, 2018, and September 30, 2020.

Demographic data, including age, gender, and disease duration, were collected for 43 individuals with ataxia. Forty-three healthy controls with no neurological or ocular disease were included in the study.

Ataxia severity was determined based on the Scale for the Assessment and Rating of Ataxia (SARA).[22] The SARA ranges from 0 (no ataxia) to 40 (most severe ataxia) based on the evaluation of eight items for gait capacity, static balance, sitting, speech disturbance, and limb kinetic functions.

Each participant underwent best-corrected visual acuity (BCVA) testing using retroilluminated Early Treatment Diabetic Retinopathy Study (ETDRS) charts at 4-meter distance (Precision Vision, Woodstock, IL). Exclusion criteria included high myopia (<−7 diopters), any concomitant ocular disease or ocular surgery in the past 3 months, uncontrolled arterial hypertension, and uncontrolled diabetes mellitus.

OCT-A Imaging

OCT-A imaging was performed without pupil dilation using a spectral domain OCT-A device (AngioVue, RTVue XR Avanti SD-OCT, Optovue, Fremont, CA). This device operates with a scan rate of 70,000 A-scans/s, a scan beam wavelength of 840 ± 10 nm, and a bandwidth of 45 nm.

Volumetric 6 × 6 mm high-definition macular scans centered at the fovea and 4.5 × 4.5 mm high-definition optic nerve head (ONH) scans were captured. The software of the device automatically segments macular scans into superficial retinal vascular plexus (SVP), spanning from the internal limiting membrane to the lower border of the inner plexiform layer (IPL), and deep retinal vascular plexus (DVP), extending from the inner nuclear layer (INL) to the outer plexiform layer (OPL), as well as the outer retina and choriocapillaris. In the ONH scans, only the SVP was depicted. In addition, vessel densities of the whole image, parafovea, and perifovea applying a grid overlay according to the standard ETDRS subfields, peripapillary region, inside the ONH, and the foveal avascular zone (FAZ) were calculated and identified automatically. The accuracy of automatic segmentation was checked, and manual correction was performed if needed.

Vessel density was defined as the proportion of vessel area with detectable blood flow over the total area measured. Only images with sufficient signal strength (≥60) and scan quality (≥6/10) and without motion artifacts (no or only minimal banding/quilting) were included.[23,24]

Read-out parameters of the OCT-A included vessel density of the superficial and deep macular plexuses, vessel density of the radial peripapillary capillary (RPC) network, and capillary density inside the optic nerve head (cdONH) and FAZ area.

Structural OCT Imaging

Structural OCT imaging was performed using a spectral domain OCT (Spectralis, Heidelberg Engineering, Heidelberg, Germany). Volumetric macular scans were

acquired with a scanning protocol of 20 × 20°, 1024 scans, and 97 sections in high-resolution mode to assess added up foveal and parafoveal volumes of the macular RNFL, GCL, IPL, INL, OPL, and outer nuclear layer. In addition, a circumferential peripapillary scan was captured to measure the peripapillary RNFL (pRNFL) thickness with all its subdivisions, including global (G), nasal (N), nasal inferior (NI), temporal inferior (TI), temporal (T), temporal superior (TS), and nasal superior (NS). The accuracy of automatic segmentation was checked, and manual correction was performed in case of segmentation errors.

Data Analysis

When available, data from both eyes of each subject were included, and for the fixed effect analyses a mean value was calculated. All subjects diagnosed clinically with ataxia using the SARA were initially included in the general/overall ataxia cohort and compared with the control group. Subsequently, based on genotyping, six separate ataxia subgroups (SCA1, SCA2, SCA3, SCA6, FRDA, and MSA-C) were established and compared with randomly selected age-matched (±3 years; 1:2 matching) control groups.

Analysis of variance was applied to compare the general ataxia cohort with the cohort of healthy subjects. In an age-matched (±3 years; 1 case to 2 controls) subgroup analysis by ataxia type, Shapiro–Wilk tests were performed to assess the normality of the data. When the data were compliant with the normality assumption, the independent *t* test (2-tailed) was used. If the values were not normally distributed however, the Mann-Whitney *U* test (2-tailed) was applied.

To challenge and confirm the outcomes of the fixed effect analyses for statistically significant variables, mixed effect model analyses were performed with right- and left-eye variables as repeated measures outcome and diagnosis and hemisphere (right eye/left eye) as well as the interaction between diagnosis and hemisphere as independent variables with the effects blocked within subjects.

The relationships between OCT-A and OCT parameters with clinical characteristics were explored using Pearson's and Spearman's partial correlation analyses adjusted by age among all ataxia subjects. Correlation analyses were performed separately for right and left eyes.

Statistical significance was set at $P < 0.05$. Statistical analyses and graphical representation were performed using SPSS software version 26.0.0.0 (SPSS Inc., Chicago, IL) and GraphPad Prism version 8.4.3 (GraphPad Software, San Diego, CA). The mixed effect models were computed using R software with the library "lmerTest" version 3.3.1 (R Foundation for Statistical Computing, Vienna, Austria).

Data Availability

The data that support the findings of this study are available from the corresponding author on reasonable institutional request.

Results

Patient Demographics and Disease Characteristics

Forty-three subjects with clinically confirmed ataxia were included: 4 with SCA1, 1 with SCA2, 13 with SCA3, 12 with SCA6, 6 with FRDA, and 7 with MSA-C.

TABLE 1 *Demographic and clinical characteristics of patients with SCA1, SCA2, SCA3, SCA6, MSA-C, and FRDA*

	SCA1 (n = 4)	SCA2 (n = 1)	SCA3 (n = 13)	SCA6 (n = 12)
Age (y)	39.0 ± 2.71	53.0	52.08 ± 9.64	62.08 ± 10.35
Gender (M/F)	2:2	1:0	7:6	11:1
BCVA	0.04 ± 0.08	0.00	0.01 ± 0.08	0.07 ± 0.16
Disease duration (y)	3.75 ± 0.96	10.0	7.60 ± 4.35	8.33 ± 4.41
SARA score	11.75 ± 3.52	12	8.38 ± 3.89	11.18 ± 5.93
		MSA-C (n = 7)		FRDA (n = 6)
Age (y)		58.14 ± 6.57		45.33 ± 13.13
Gender (M/F)		3:4		3:3
BCVA		0.11 ± 0.15		0.01 ± 0.07
Disease duration (y)		5.60 ± 1.82		18.60 ± 12.14
SARA score		14.07 ± 4.60		19.33 ± 7.67

Data represent means ± standard deviation.
Abbreviations: SCA1, spinocerebellar ataxia type 1; SCA2, spinocerebellar ataxia type 2; SCA3, spinocerebellar ataxia type 3; SCA6, spinocerebellar ataxia type 6; MSA-C, multisystem atrophy type C; FRDA, Friedreich's ataxia; BCVA, best-corrected visual acuity in LogMAR; SARA, Scale for the Assessment and Rating of Ataxia.

TABLE 2 *Vascular density, ganglion cell layer volume, and temporal peripapillary retinal nerve fiber layer thickness in ataxia and healthy control cohorts*

Parameter	Ataxia (n = 43)	Controls (n = 43)	*P*-value
nSVP (%)	52.49 ± 2.98	53.81 ± 2.36	0.03
Peripapillary vessel density (%)	50.12 ± 2.24	51.63 ± 2.58	0.005
Capillary density optic nerve head (%)	48.57 ± 3.77	51.46 ± 3.66	0.0005
Ganglion cell layer (mm^3)	0.323 ± 0.03	0.336 ± 0.03	0.04
Retinal nerve fiber layer temporal (μm)	67.72 ± 8.72	72.49 ± 11.12	0.04

Optical coherence tomography angiography (OCT-A) imaging was performed without pupil dilation using a spectral domain device of AngioVue, RTVue XR Avanti SD-OCT, Optovue. Vessel density was defined as the proportion of vessel area with detectable blood flow over the total area measured. Only images without motion artifacts were included. Read-out parameters included vessel density of the superficial and deep macular plexuses, vessel density of the radial peripapillary capillary network, the capillary density inside the ONH, and foveal avascular zone area.

Structural OCT imaging was performed using a spectral domain device of Spectralis (Heidelberg Engineering) to assess added-up foveal and parafoveal volumes of the macular retinal nerve fiber layer (mRNFL), ganglion cell layer, inner plexiform layer, inner nuclear layer, outer plexiform layer, and outer nuclear layer. In addition, a circumferential peripapillary scan was captured to measure the peripapillary RNFL thickness with all its subdivisions, including global (G), nasal (N), nasal inferior (NI), temporal inferior (TI), temporal (T), temporal superior (TS), and nasal superior (NS).

Data represent means ± standard deviation, with *P*-values derived from the respective analysis of variance analyses revealing significant differences between cohorts. Comparison of all remaining parameters measured using OCT or OCT-A and the aforementioned data did not reveal significant differences.

Significant at $P < 0.05$.

Abbreviation: nSVP, nasal superficial vascular plexus (combined nasal parafovea and nasal perifovea average).

The mean age was 53.7 ± 11.7 years; 27 (62.8%) were men. For the healthy control cohort, the mean age was 55.6 ± 13.7 years; 29 (67.4%) were women. BCVA of patients with ataxia and healthy controls was LogMar 0.04 ± 0.12 and –0.03 ± 0.12, respectively. The mean duration of ataxia symptoms was 8.7 ± 7.1 years. The

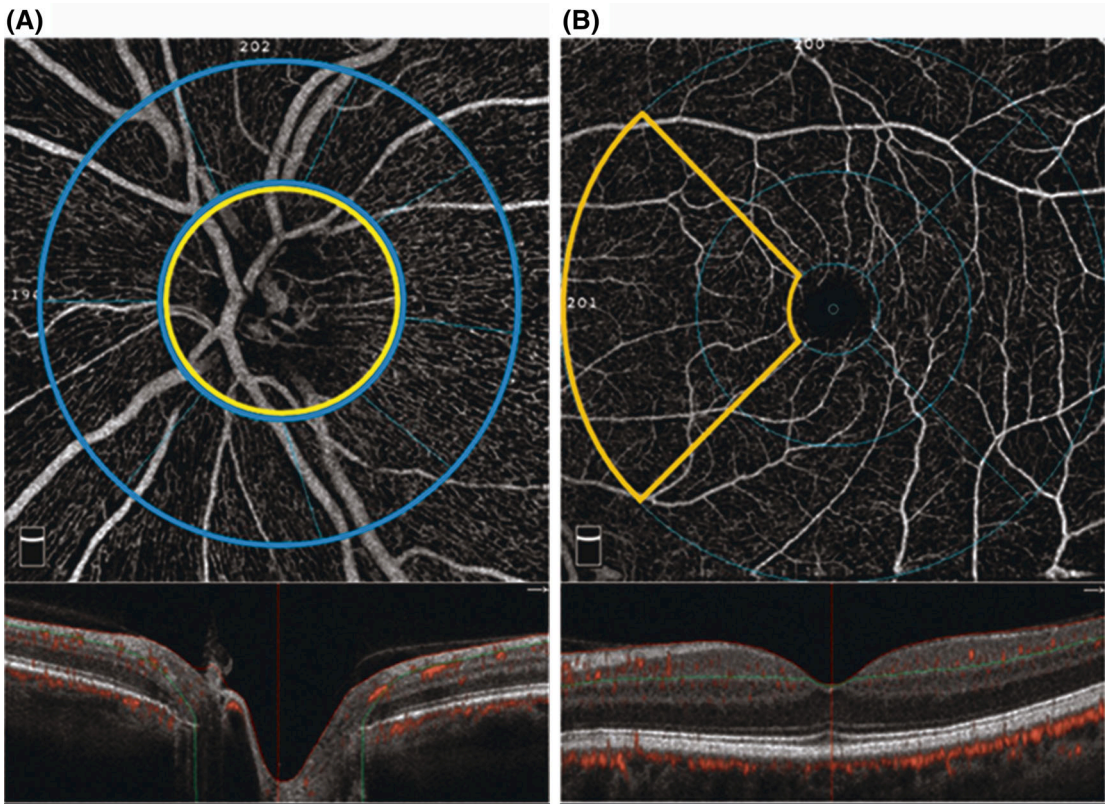

FIG. 1. Image analysis of OCT angiography of the peripapillary, parafoveal, and perifoveal areas of the left eye from a SCA6 patient. (**A**) Radial peripapillary capillary network (highlighted area within blue circles, upper en face image) and capillary density inside the optic nerve head (highlighted area within yellow circle, upper en face image) vasculature within the internal limiting membrane (red line, lower B-scan image) and the retinal nerve fiber layer (green line, lower B-scan image). (**B**) Superficial parafoveal (inner circular area outside of foveal avascular zone, upper en face image) and perifoveal (outer circular area, upper en face image) capillary network extending from the internal limiting membrane (red line, lower B-scan image) to the outer boundary of the inner plexiform layer (green line, lower B-scan image). Nasal region (combined parafoveal and perifoveal average) of the nasal superficial vascular plexus (nSVP) highlighted in orange.

extent of ataxia as assessed by the SARA was 12.1 ± 6.1. The mean age, gender, BCVA, disease duration, and total SARA score of individual ataxia subgroups are provided in Table 1. The age of onset was defined as the first onset of gait disturbances, and disease duration was calculated accordingly.

Ocular Imaging

In total, 8 eyes of 4 SCA1 subjects, 4 eyes of 2 SCA2 subjects, 34 eyes of 17 SCA3 subjects, 32 eyes of 16 SCA6 subjects, 20 eyes of 10 FRDA subjects, 18 eyes of 9 MSA-C subjects, and 108 eyes of 54 healthy control subjects were enrolled and imaged in this study (Figure S1). Two eyes of 1 SCA2 subject, 8 eyes of 4 SCA3 subjects, 8 eyes of 4 SCA6 subjects, 8 eyes of 4 FRDA subjects, 4 eyes of 2 MSA-C subjects, and 22 eyes of 11 healthy controls were excluded. In ataxia subjects, 20 eyes were excluded due to reduced scan quality and motion artifact. In addition, six eyes with incidental findings of dry age-related macular degeneration (AMD) and two eyes with central serous retinopathy were not included in the study. In the control group, 10 eyes had to be omitted from further analysis because of insufficient scan quality and motion artifact as well as 12 eyes due to an incidental finding of dry AMD. Finally, 82 eyes of 43 ataxia subjects and 85 eyes of 43 controls were included in the analyses.

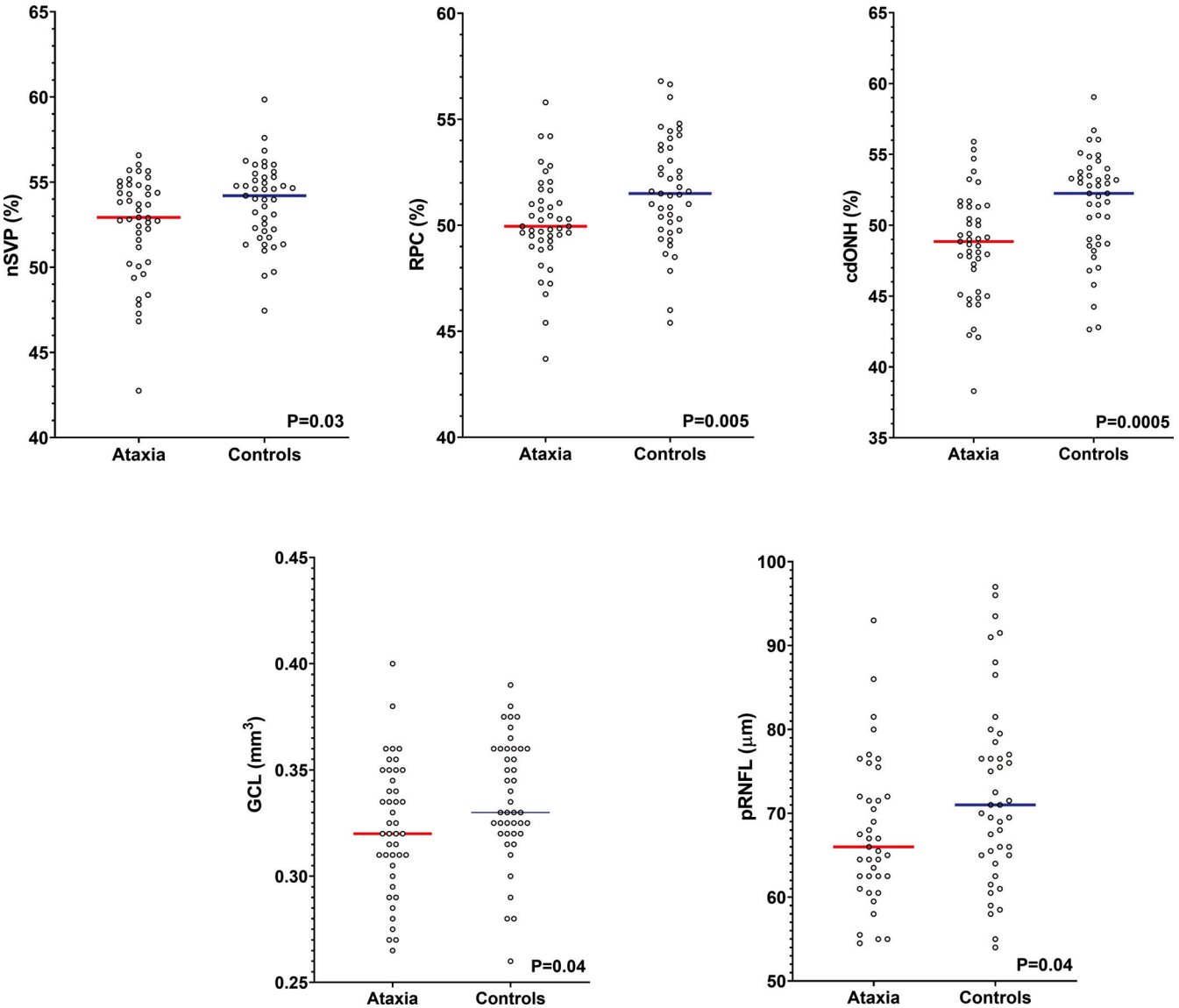

FIG. 2. Graphical representation of the data subjected to the fixed effect model analyses for OCT-A and OCT parameters in ataxia and healthy control cohorts. Fixed effect model analyses were performed on 21 variables, 5 of which had become significant. These variables were nSVP (nasal superficial vascular plexus, combined nasal parafovea and nasal perifovea average), RPC (vessel density radial peripapillary capillary network), cdONH (capillary density inside optic nerve head), GCL (ganglion cell layer volume), and pRNFL (temporal peripapillary retinal nerve fiber layer thickness). Data are presented as scatterplots of means from both eyes of each subject. Significant at $P < 0.05$.

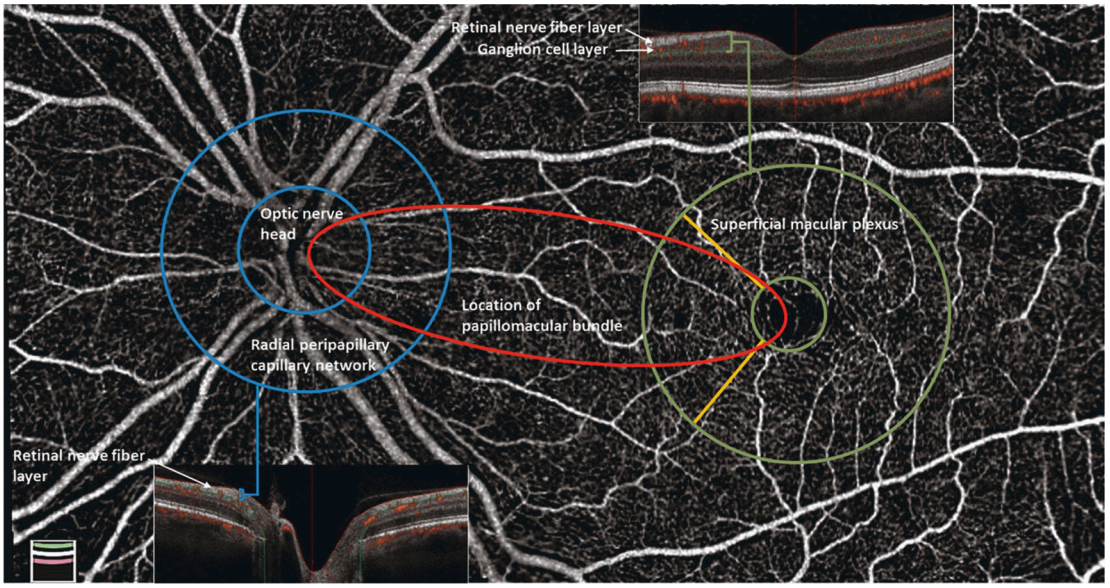

FIG. 3. Schematic illustration of affected regions within the retina of ataxia patients. En face OCT angiography montage image highlighting vessel density inside the optic nerve head (area within inner blue circle), peripapillary region (area between inner and outer blue circles), and nasal region of the superficial macular plexus (area between orange and green lines). Area within red zone marks location of papillomacular bundle. Area between green circles represents the parafoveal and perifoveal superficial plexus. Horizontal B-scans in right-upper and left-lower part of montage image highlight location of the retinal nerve fiber layer, ganglion cell layer, and the depicted retinal vasculature (between upper-red and lower-green lines).

When comparing all ataxia patients (n = 43) with healthy controls (n = 43) using fixed effect analysis, subjects with ataxia exhibited significantly reduced vessel density in the RPC network ($P = 0.005$), cdONH ($P < 0.001$), nasal superficial vascular plexus (nSVP) ($P = 0.03$), reduced GCL ($P = 0.04$), and reduced temporal pRNFL thickness ($P = 0.04$) (Table 2; Figs. 1 and 2). A mixed effect model analysis in R with left- and right-eye variables as repeated measures outcome and diagnosis and hemisphere (left/right) as well as the interaction between diagnosis and hemisphere as independent variables with the effects blocked within subjects confirmed the outcomes of the fixed effect model analyses for RPC ($P = 0.002$), cdONH ($P = 0.01$), nSVP ($P = 0.034$), GCL ($P = 0.0408$), and temporal pRNFL ($P = 0.0177$), revealing that there was a significant effect of diagnosis for these five outcomes and no interaction between hemisphere and diagnosis on the outcome measures. Detailed results of the linear mixed effect model analysis for statistically significant parameters of the fixed effect analyses are provided in Figure S2. Only for GCL ($P = 0.02$) and temporal pRNFL ($P = 0.04$) was an additional main effect of hemisphere (larger values in right vs. left eye) detected.

When comparing ataxia diagnostic subtypes, subjects with SCA1 exhibited a significant decrease in GCL ($P = 0.04$), increase in OPL ($P = 0.01$), and reduced nasal-superior pRNFL thickness ($P = 0.03$). Subjects with SCA3 exhibited significantly reduced vessel density in the RPC network ($P = 0.007$), cdONH ($P = 0.02$), and reduced GCL ($P = 0.03$) (Table S1). The SCA6 cohort was characterized by diminished vessel density in the cdONH ($P = 0.001$) and nSVP ($P = 0.04$). The FRDA cohort exhibited a significant reduction in vessel density in the RPC network ($P = 0.04$), cdONH ($P = 0.002$), and nSVP ($P = 0.01$). The MSA-C cohort presented with reduced cdONH ($P = 0.04$) when compared with respective controls (Table S1; Fig. 3).

For OCT-A parameters, cdONH (right eye: $r = -0.326$, $P = 0.049$) was correlated significantly with the SARA score as was the nSVP (right eye: $r = -0.445$, $P = 0.02$; left eye: $r = -0.404$, $P = 0.03$) with disease duration (Table S2). No significant correlations were found for OCT parameters.

Discussion

We found a distinct pattern of reduced retinal vessel density in degenerative ataxias using OCT-A imaging pertaining to the ONH region and the nasal portion of the macular SVP.

These findings, together with structural changes in inner retinal layers detected using structural OCT imaging, enable new insights into mechanisms of neurodegeneration related to a possible coupling of neuronal damage in the retina and retinal microvascular changes in neurodegenerative ataxias.[4-13]

Our results are particularly intriguing because retinal vascular alterations, so far documented in AD, in which

cerebral amyloid angiopathy is a known pathogenic factor, have neither been reported nor suspected in degenerative ataxias.[15,16] To our knowledge, our study is the first to perform OCT-A in combination with structural OCT imaging simultaneously in subjects with inherited and sporadic ataxias allowing for an insight into ongoing retinal degeneration at the cellular and microvascular levels at the same time.

The microvasculature of the inner retina is divided into four major plexuses originating from the central retinal artery. These are the superficial retinal vascular plexus (SVP), the more superficial radial peripapillary capillary plexus (RPCP), the deeper positioned intermediate capillary plexus (ICP), and the deep retinal capillary plexus (DCP).[25-28] RPCP and SVP are grouped together as the superficial vascular complex (SVC) and ICP and DCP as the deep vascular complex. The SVC forms a particularly dense vascular network in the peripapillary region characterized by decreasing vessel density with distance from the ONH along the maculopapillary axis.[25] The RPCP is supplied by feeder vessels from the SVP and consists of capillaries running in parallel with axons in the RNFL.[25-27]Our study revealed changes involving primarily the retinal RPC vascular network, cdONH, and nSVP. These findings were accompanied by peripapillary RNFL thinning in the temporal region and reduction in GCL volume, indicating a possible predilection of neurodegenerative processes in the retina of ataxia patients occurring at the ONH and extending toward the papillomacular bundle.[7] This is in accordance with morphological evidence and studies using retinal OCT imaging in SCA1, Parkinson's disease, and Huntington's disease (HD), which found that parvocellular retinal ganglion cell loss is reflected by temporal RNFL thinning.[7,29-31] These findings resemble changes discovered in mitochondrial optic neuropathies, such as Leber's hereditary optic neuropathy and dominant optic atrophy, characterized by pathological involvement of thinly myelinated axons of the papillomacular bundle resulting in temporal optic disc pallor.[7,29-34]

It remains unclear whether vascular changes precede structural changes such as a reduction in RNFL thickness or GCL volume or vice versa. It could be hypothesized that neurodegeneration primarily occurring at the ONH and papillomacular bundle leads to reduced metabolic demand in these regions, requiring less perfusion and consequently resulting in diminished blood supply from the SVP.[35]

Cell death, axon loss, and RNFL thinning in the retina may not be detectable in very early stages of ataxias. Alternatively, ataxia patients may have anatomically distinct RPCPs compared to healthy subjects, indicating that, for instance, fewer and/or narrower feeder vessels from the SVP could result in reduced blood supply and RNFL thinning over time. Reduced vessel density in the RPCP could therefore be regarded as a cause or consequence of thinning RNFL. However, it could also be attributed to structural changes in retinal tissue in the peripapillary region caused by glial fibrillary degeneration around the ONH.[36-38] Changes in vessel density inside and in the vicinity of the ONH may indicate the starting point of neurodegeneration and represent a reflection of ischemia in the retina in ataxia patients.

Vessel density in the DVP was not significantly reduced and remained homogenous in the ataxia cohorts. The widely anastomotic organization of the DVP may be able to mitigate the effect of decreased blood supply from the SVP and preserve sufficient oxygen supply to retinal layers in its vicinity, namely the OPL and INL. These retinal layers generally have a lower arterial oxygen partial pressure (PaO_2) tissue level compared to anatomically more superiorly located layers such as the RNFL, GCL, and IPL.[39,40] None of our patient cohorts exhibited significantly reduced volume changes in the OPL or INL.

Alternatively, it could be hypothesized that microvascular breakdown primarily occurring in the retinal SVC, encompassing the nSVP, RPC network, and cdONH, leads to reduced metabolic supply in the regions requiring the highest perfusion and consequently results in the degeneration of neurons in the GCL and loss of axons in the peripapillary RNFL.

Our findings demonstrate that distinct retinal vascular changes are present in degenerative ataxias. SCAs are polyglutamine diseases morphologically characterized by the accumulation of abnormal intracellular protein aggregates in neurons and along their axons.[41] These aggregate species can impair mitochondrial function as well as cause alterations in the chaperone and ubiquitin proteasome system ultimately affecting cellular metabolism leading to an increased sensitivity to oxidative stress.[42] Such protein aggregates can be expressed by brain blood vessels and may disrupt the blood–brain barrier in SCA3.[43]

It cannot be ruled out, therefore, that such aggregates could also be present in the retinal vasculature, even though not detectable using OCT-A and OCT. In addition, MSA-C is a synucleinopathy with the formation of intracellular α-synuclein aggregates.[3,44,45] The exact function of monomeric α-synuclein is still not clearly understood. The possibility of antioxidant and antiapoptotic properties has been suggested.[46-48]

If such deposits reach or form in retinal tissue, impaired metabolic activity could be a consequence. Furthermore, FRDA is characterized by reduced and impaired intracellular frataxin protein levels, resulting in impaired mitochondrial function and increased levels of reactive oxygen species.[49,50] However, no accumulation of abnormal intracellular protein aggregates in neurons has been detected in FRDA.

Thus far, large-scale OCT-A studies have been performed in patients suffering from AD (n = 39) and mild

cognitive impairment (n = 37), suggesting β-amyloid as a cause for reduced vessel density in the retina.[16] We hypothesize that polyglutamines and other protein aggregates may act as a similar culprit in genetic and certain sporadic forms of ataxia affecting cellular metabolic function, eventually leading to protracted hypoxia, compensated for by redirecting or withholding blood supply from metabolically less-critical or less-affected retinal regions. Alternatively, ganglion cells and their axons could be impaired, causing a decrease in metabolic activity and thus size and require a vasculature with less density. In particular, alterations in the RPC network, cdONH, and the nSVP could be regarded as likely indicators of these processes and should be closely monitored to clarify the chain of events.

The advantages of this study are the large sample size for ataxias; the comprehensive assessment of both subjects with ataxia and healthy controls, including the exclusion of ocular pathology; and the extensive retinal imaging employing both structural OCT and OCT-A. Retinal imaging was quality controlled, and automated segmentation was manually corrected if needed, which increased the quality of the collected data. Implementing the study at only one site reduced variability. The limitations of the study include the lack of longitudinal data and its explorative nature.

In conclusion, distinct microvascular retinal changes can be detected using OCT-A imaging in inherited and sporadic neurodegenerative ataxias. Experience obtained in ataxia cohorts can guide other studies using OCT-A technology in combination with structural OCT imaging in various other neurodegenerative disorders, particularly those dependent on protein storage defects such as AD, frontotemporal dementia, or HD.

These observations indicate that degeneration may target both neuronal and vascular elements in the retina and possibly other parts of the brain and spinal cord to induce neurological decline in ataxias. Thus, the clinical signs in ataxias may be attributed to the demise of various cellular populations in the central nervous system involving neuronal and vascular networks.

These conclusions may be relevant to ataxia therapy and perhaps other neurodegenerative diseases. The experimental symptomatic therapies of ataxias such as those modulating ion channels in cerebellar circuitries relied exclusively on the neuronal component of degeneration.[51] Our results indicate that therapeutic strategies for ataxias should be complemented by measures concurrently involving neurons and blood vessels to effectively reduce neuronal injury and the following neurological disability. ●

Acknowledgments: Open Access funding enabled and organized by Projekt DEAL.

Statement of Ethics

Informed consent was obtained from the subjects before enrollment in the study. The study was approved by the Institutional Review Board of the University of Bonn, Bonn, Germany, and all procedures adhered to the tenets of the Declaration of Helsinki.

Data Availability Statement

The data that support the findings of this study are available from the corresponding author upon reasonable institutional request.

References

1. Pandolfo M. Friedreich ataxia. Arch Neurol 2008;65:1296–1303.
2. Klockgether T, Mariotti C, Paulson HL. Spinocerebellar ataxia. Nat Rev Dis Primers 2019;5:24.
3. Fanciulli A, Wenning GK. Multiple-system atrophy. N Engl J Med 2015;372:249–263.
4. Mendoza-Santiesteban CE, Palma JA, Martinez J, et al. Progressive retinal structure abnormalities in multiple system atrophy. Mov Disord 2015;30:1944–1953.
5. Mendoza-Santiesteban CE, Gabilondo I, Palma JA, Norcliffe-Kaufmann L, Kaufmann H. The retina in multiple system atrophy: systematic review and meta-analysis. Front Neurol 2017;8:206.
6. Oertel FC, Zeitz O, Rönnefarth M, et al. Functionally relevant maculopathy and optic atrophy in spinocerebellar ataxia type 1. Mov Disord Clin Pract 2020;7:502–508.
7. Stricker S, Oberwahrenbrock T, Zimmermann H, et al. Temporal retinal nerve fiber loss in patients with spinocerebellar ataxia type 1. PLoS One 2011;6:e23024.
8. Park JY, Joo K, Woo SJ. Ophthalmic manifestations and genetics of the polyglutamine autosomal dominant spinocerebellar ataxias: a review. Front Neurosci 2020;14:892.
9. lvarez G, Rey A, Sanchez-Dalmau B, Muñoz E, Ríos J, Adán A. Optical coherence tomography findings in spinocerebellar ataxia-3. Eye 2013;27:1376–1381.
10. Pula JH, Towle VL, Staszak VM, Cao D, Bernard JT, Gomez CM. Retinal nerve fibre layer and macular thinning in spinocerebellar ataxia and cerebellar multisystem atrophy. Neuroophthalmology 2011;35:108–114.
11. Spina Tensini F, Sato MT, Shiokawa N, Ashizawa T, Teive HAG. A comparative optical coherence tomography study of spinocerebellar ataxia types 3 and 10. Cerebellum 2017;16:797–801.
12. Dağ E, Örnek N, Örnek K, Erbahçeci-Timur IE. Optical coherence tomography and visual field findings in patients with Friedreich ataxia. J Neuroophthalmol 2014;34:118–121.
13. Martinez-Lapiscina EH, Arnow S, Wilson JA, et al. Retinal thickness measured with optical coherence tomography and risk of disability worsening in multiple sclerosis: a cohort study. Lancet Neurol 2016;15:574–584.
14. Bulut M, Kurtuluş F, Gözkaya O, et al. Evaluation of optical coherence tomography angiographic findings in Alzheimer's type dementia. Br J Ophthalmol 2018;102:233–237.
15. Yoon SP, Grewal DS, Polascik B, et al. Comparison of retinal microvasculature and neurodegenerative changes among Alzheimer's disease, mild cognitive impairment, and controls. Invest Ophthalmol Vis Sci 2018;59:2818–2818.
16. Yoon SP, Grewal DS, Thompson AC, et al. Retinal microvascular and neurodegenerative changes in Alzheimer's disease and mild cognitive impairment compared with control participants. Ophthalmol Retina 2019;3:489–499.
17. Zhang YS, Zhou N, Knoll BM, et al. Parafoveal vessel loss and correlation between peripapillary vessel density and cognitive performance in amnestic mild cognitive impairment and early Alzheimer's disease on optical coherence tomography angiography. PLoS One 2019;14:e0214685.

18. Kwapong WR, Ye H, Peng C, et al. Retinal microvascular impairment in the early stages of Parkinson's disease. Invest Ophthalmol Vis Sci 2018;59:4115–4122.

19. O'Bryhim BE, Apte RS, Kung N, Coble D, Van Stavern GP. Association of preclinical Alzheimer disease with optical coherence tomographic angiography findings. JAMA Ophthalmol 2018;136:1242–1248.

20. Nelis P, Kleffner I, Burg MC, et al. OCT-angiography reveals reduced vessel density in the deep retinal plexus of CADASIL patients. Sci Rep 2018;8:8148.

21. Spaide RF, Fujimoto JG, Waheed NK, Sadda SR, Staurenghi G. Optical coherence tomography angiography. Prog Retin Eye Res 2018;64:1–55.

22. Schmitz-Hübsch T, du Montcel ST, Baliko L, et al. Scale for the assessment and rating of ataxia: development of a new clinical scale. Neurology 2006;66:1717–1720.

23. Lauermann JL, Woetzel AK, Treder M, et al. Prevalences of segmentation errors and motion artifacts in OCT-angiography differ among retinal diseases. Graefes Arch Clin Exp Ophthalmol 2018;256:1807–1816.

24. Lauermann JL, Treder M, Heiduschka P, Clemens CR, Eter N, Alten F. Impact of eye-tracking technology on OCT-angiography imaging quality in age-related macular degeneration. Graefes Arch Clin Exp Ophthalmol 2017;255:1535–1542.

25. Campbell JP, Zhang M, Hwang TS, et al. Detailed vascular anatomy of the human retina by projection-resolved optical coherence tomography angiography. Sci Rep 2017;7:42201.

26. Fouquet S, Vacca O, Sennlaub F, Paques M. The 3D retinal capillary circulation in pigs reveals a predominant serial organization. Invest Ophthalmol Vis Sci 2017;58:5754–5763.

27. Jia Y, Simonett JM, Wang J, et al. Wide-field OCT angiography investigation of the relationship between radial peripapillary capillary plexus density and nerve fiber layer thickness. Invest Ophthalmol Vis Sci 2017;58:5188–5194.

28. Cuenca N, Ortuño-Lizarán I, Sánchez-Sáez X, et al. Interpretation of OCT and OCTA images from a histological approach: clinical and experimental implications. Prog Retin Eye Res 2020;77:100828.

29. La Morgia C, Di Vito L, Carelli V, Carbonelli M. Patterns of retinal ganglion cell damage in neurodegenerative disorders: parvocellular vs magnocellular degeneration in optical coherence tomography studies. Front Neurol 2017;8:710.

30. La Morgia C, Ross-Cisneros FN, Sadun AA, Carelli V. Retinal ganglion cells and circadian rhythms in Alzheimer's disease, Parkinson's disease, and beyond. Front Neurol 2017;8:162.

31. Kersten HM, Danesh-Meyer HV, Kilfoyle DH, Roxburgh RH. Optical coherence tomography findings in Huntington's disease: a potential biomarker of disease progression. J Neurol 2015;262:2457–2465.

32. Carelli V, Ross-Cisneros FN, Sadun AA. Mitochondrial dysfunction as a cause of optic neuropathies. Prog Retin Eye Res 2004;23:53–89.

33. Yu-Wai-Man P, Griffiths PG, Chinnery PF. Mitochondrial optic neuropathies - disease mechanisms and therapeutic strategies. Prog Retin Eye Res 2011;30:81–114.

34. Pan BX, Ross-Cisneros FN, Carelli V, et al. Mathematically modeling the involvement of axons in Leber's hereditary optic neuropathy. Invest Ophthalmol Vis Sci 2012;53:7608–7617.

35. Higashiyama T, Nishida Y, Ohji M. Optical coherence tomography angiography in eyes with good visual acuity recovery after treatment for optic neuritis. PLoS One 2017;12:e0172168.

36. Kim JH, Lukowicz A, Qu W, Johnson A, Cvetanovic M. Astroglia contribute to the pathogenesis of spinocerebellar ataxia Type 1 (SCA1) in a biphasic, stage-of-disease specific manner. Glia 2018;66:1972–1987.

37. Cerrato V. Cerebellar astrocytes: much more than passive bystanders in ataxia pathophysiology. J Clin Med 2020;9:757.

38. Zeitlberger AM, Thomas-Black G, Garcia-Moreno H, et al. Plasma markers of neurodegeneration are raised in Friedreich's ataxia. Front Cell Neurosci 2018;12:366.

39. Linsenmeier RA, Zhang HF. Retinal oxygen: from animals to humans. Prog Retin Eye Res 2017;58:115–151.

40. Tan PE, Yu PK, Balaratnasingam C, et al. Quantitative confocal imaging of the retinal microvasculature in the human retina. Invest Ophthalmol Vis Sci 2012;53:5728–5736.

41. Fan HC, Ho LI, Chi CS, et al. Polyglutamine (PolyQ) diseases: genetics to treatments. Cell Transplant 2014;23:441–458.

42. Matos CA, de Almeida LP, Nóbrega C. Machado-Joseph disease/spinocerebellar ataxia type 3: lessons from disease pathogenesis and clues into therapy. J Neurochem 2019;148:8–28.

43. Duarte Lobo D, Nobre RJ, Oliveira Miranda C, et al. The blood-brain barrier is disrupted in Machado-Joseph disease/spinocerebellar ataxia type 3: evidence from transgenic mice and human post-mortem samples. Acta Neuropathol Commun 2020;8:152.

44. Galvin JE, Lee VM, Trojanowski JQ. Synucleinopathies: clinical and pathological implications. Arch Neurol 2001;58:186–190.

45. Roncevic D, Palma JA, Martinez J, et al. Cerebellar and parkinsonian phenotypes in multiple system atrophy: similarities, differences and survival. J Neural Transm 2014;121:507–512.

46. Jin H, Kanthasamy A, Ghosh A, et al. α-Synuclein negatively regulates protein kinase Cd expression to suppress apoptosis in dopaminergic neurons by reducing p300 histone acetyltransferase activity. J Neurosci 2011;31:2035–2051.

47. Zhu M, Qin ZJ, Hu D, Munishkina LA, Fink AL. Alpha-synuclein can function as an antioxidant preventing oxidation of unsaturated lipid in vesicles. Biochemistry 2006;45:8135–8142.

48. Latchoumycandane C, Anantharam V, Kitazawa M, Yang Y, Kanthasamy A, Kanthasamy AG. Protein kinase Cdelta is a key downstream mediator of manganese-induced apoptosis in dopaminergic neuronal cells. J Pharmacol Exp Ther 2005;313:46–55.

49. Pandolfo M. Molecular pathogenesis of Friedreich ataxia. Arch Neurol 1999;56:1201–1208.

50. González-Cabo P, Palau F. Mitochondrial pathophysiology in Friedreich's ataxia. J Neurochem 2013;126:53–64.

51. Ashizawa T, Öz G, Paulson HL. Spinocerebellar ataxias: prospects and challenges for therapy development. Nat Rev Neurol 2018;14:590–605.

Supporting Data

Additional Supporting Information may be found in the online version of this article at the publisher's web-site.